Inflammation Research (2019) 68:677–689
https://doi.org/10.1007/s00011-019-01251-x

Inflammation Research

ORIGINAL RESEARCH PAPER

High-mobility group box-1 inhibition stabilizes intestinal permeability through tight junctions in experimental acute necrotizing pancreatitis

Luqiao Huang[1] · Dianliang Zhang[1] · Wenli Han[3] · Chunbao Guo[2,4]

Received: 6 March 2019 / Revised: 22 May 2019 / Accepted: 24 May 2019 / Published online: 28 May 2019
© Springer Nature Switzerland AG 2019

Abstract

Background In acute necrotizing pancreatitis (ANP), bacterial translocation (BT) from the gastrointestinal tract is the essential pathogenesis in the development of septic complications. Although high-mobility group box-1 (HMGB1) is associated with BT and organ dysfunction in ANP, the mechanism of HMGB1 in the intestinal barrier dysfunction and BT has not been well addressed. In this study, we intend to address the role of HMGB1 in ANP involving BT and intestinal barrier dysfunction.

Methods Experimental ANP was achieved in male Sprague–Dawley rats through a retrograde injection of taurocholate into the common biliopancreatic duct following a laparotomy operation. HMGB1 blockade intervention was conducted with a subcutaneous injection of anti-HMGB1 antibody immediately before the laparotomy procedure. Twenty-four hours after ANP induction, pancreatic and intestinal tissues and blood samples were collected for a histopathological assessment and lipid peroxidation or glutathione (GSH) evaluation. AP-induced barrier dysfunction was determined by an intestinal permeability assessment. Tight junction proteins and autophagy regulators were investigated by western blotting, immunohistological analysis and confocal immunofluorescence imaging.

Results ANP developed as indicated by microscopic parenchymal necrosis and fat necrosis, which were associated with intestinal mucosal barrier dysfunction. HMGB1 inhibition played a protective role in intestinal mucosal barrier dysfunction, protected against microbiome changes in ANP, and relieved intestinal oxidative stress. Additionally, HMGB1 inhibition attenuated intestinal permeability; preserved the expression of TJs, such as claudin-2 and occludin; and decreased autophagy. Furthermore, the autophagy regulator LC3 and TJ protein claudin-2 were both upregulated in ANP according to dual immunofluorescence analysis.

Conclusion HMGB1 inhibition ameliorated the severity of experimental ANP though beneficial effects on BT, mainly involving in TJ function.

Keywords High-mobility group box-1 · Intestinal permeability · Tight junctions · Autophagy · Acute necrotizing pancreatitis

Abbreviations

ANP	Acute necrotizing pancreatitis
TJs	Tight junctions
HMGB1	High-mobility group box-1
MDA	Malonaldehyde
SOD	Superoxide dismutase
MPO	Myeloperoxidase
GSH	Glutathione
GSSG	Oxidized glutathione
MLN	Mesenteric lymph node

Responsible Editor: John Di Battista.

✉ Wenli Han
872250656@qq.com

✉ Chunbao Guo
guochunbao@cqmu.edu.cn; guochunbao@foxmail.com

[1] Center of Colon and Rectum, Qingdao Municipal Hospital, Qingdao University, Qingdao, People's Republic of China

[2] Department of Pediatric General Surgery and Liver Transplantation, Children's Hospital, Chongqing Medical University, 136 Zhongshan 2nd Rd, Chongqing 400014, People's Republic of China

[3] Laboratory Animal Center, Chongqing Medical University, Chongqing 400014, People's Republic of China

[4] Ministry of Education Key Laboratory of Child Development and Disorders, Children's Hospital, Chongqing Medical University, Chongqing 400014, People's Republic of China

Introduction

Severe bacterial infections or sepsis complications are the main pathophysiological mechanisms of acute necrotizing pancreatitis (ANP) and are closely related to the severity of ANP [1–3]. It is generally accepted that intestinal barrier dysfunction with resulting bacterial translocation (BT) is the primary cause of systemic inflammation and sepsis complications in patients with severe acute pancreatitis [4, 5]. Barrier dysfunction was demonstrated to include damage to the structure and function of the intestinal mucosa, through which intestinal permeability is regulated by tight junctions (TJs) [6, 7]. Any factors involved in epithelial TJ disruption should contribute to barrier dysfunction and achieve the pathogenesis by which pathogens and foreign antigens cross the epithelial barrier [8, 9].

High-mobility group box-1 (HMGB1), the key inflammatory mediator, has a confirmed association with many diseases involving inflammation, such as sepsis, rheumatoid arthritis, and aortic aneurysm [10, 11]. Furthermore, HMGB1 has been found to influence the biological function of the intestinal mucosa, which plays a role in intestinal barrier injury of ANP [3, 12, 13]. HMGB1 blockade using a neutralizing antibody significantly improved the histological alterations of the pancreas in ANP and ameliorated the elevation of the serum amylase level in ANP. However, it remains unclear why HMGB1 is able to modulate the intestinal barrier function.

We previously found that the Arpin protein affects the expression of tight junction proteins and may have an impact on BT [14]. Some intermediates were also proposed to be involved in HMGB1-mediated disruption of intercellular junction proteins, such as RAGE, ERK1/2, IL-1β, TLR2, TLR4, among others. Thus, the purpose of this study was to characterize the intestinal mucosal barrier in experimental ANP and to explore the possible mechanisms of HMGB1 in the tight junctions in intestinal mucosal barrier dysfunction in rats. Determining the exact role of HMGB1 in the pathogenesis of ANP should provide a comprehensive understanding of this disease and novel targets for therapy.

Materials and methods

Animal model

The experimental protocol was approved by the Qingdao University Animal Use Committee. Male Sprague–Dawley rats weighing 280–320 g were obtained from the experimental animal center of Qingdao University. All animals were maintained in the laboratory for 1 week to acclimate to their surroundings; food was withdrawn for 12 h before the induction of ANP (rats had free access to water throughout the experimental period).

ANP was induced through a retrograde infusion of taurocholate into the biliopancreatic duct and clamping of the hepatic duct as previously reported [3]. Briefly, after anesthesia via sevoflurane (Abbott, Istanbul, Turkey) inhalation, 1 ml/kg 5% sodium taurocholate (1 ml/kg body weight; Sigma-Aldrich, St. Louis, MO, USA) was infused into the common biliopancreatic duct under laparotomy through a midline incision. In the HMGB1 blockade study, rats were randomly subjected to subcutaneous injections of the neutralizing polyclonal chicken IgY anti-HMGB1 antibody (10 mg/kg/day; Shino-Test Corporation, Tokyo, Japan) immediately before the laparotomy procedure, with the volume-matched chicken IgY antibody as a control. At 12 or 24 h after surgery, rats were killed by an intracardiac injection of pentobarbital (200 mg/kg). Blood samples (2 ml) from each rat in each group were collected from the heart before the animals were killed via a postcava puncture and split into two. Pancreas and ileum tissues adjacent to the cecum were collected and divided into two parts. One part was fixed in 4% paraformaldehyde and sectioned at 4 μm for hematoxylin and eosin (H&E) staining for histochemical analysis. The other part was frozen in liquid nitrogen for storage as frozen sections and for western blot analysis.

Morphological scoring

The same anatomical locations of pancreas and ileum tissues in each rat were assigned to histological and morphological analyses. The degrees of pancreas and intestinal mucosal injuries were scored on the histological sections by a pathologist blinded to the study conditions in 6 animals per group, 12 fields/animal. The scores of each pancreas were calculated as defined previously [15]. The scoring system for mucosal injury was graded as: normal (0); epithelial cell lifting or separation (1); necrosis to the mid-villous level (2); necrosis of the entire villus (3); and transmural necrosis (4).

Quantitative cultures and bacterial identification

To assess BT, the spleen, liver, venous blood and mesenteric lymph nodes were collected on post-operative day 1 and homogenized in sterile thioglycolate under sterile conditions as described previously [16]. The samples were plated onto blood agar plates (containing 5% sheep blood) to collect total aerobic bacteria or onto BBL brucella agar plates (containing 5% horse blood; BD) and incubated under aerobic or anaerobic conditions at 37 °C for 48–72 h, respectively, followed by the counting of colony-forming units (CFUs). Bacterial counts are expressed as colony-forming units/g tissue.

Gut microbiota analysis

Microbiota analysis was performed as previously described by our group with minor modifications [16]. Briefly, at 12 h after surgery, fecal samples were collected and subjected to DNA extraction using a fecal DNA isolation kit (Mo Bio Laboratories, USA). The V3–V5 regions of the bacterial 16S rRNA gene were amplified using a primer containing a unique 10-base barcode. Pyrosequencing data were analyzed using an open source software package, Quantitative Insight into Microbial Ecology (QIIME version 1.7.0; National Center for Biotechnology Information database accession No. SRP032495) as described previously [17]. Principal coordinate analysis (PCoA) plots were generated using the Jackknifed Beta Diversity workflow based on ten distance metrics calculated using ten subsampled operational taxonomic unit (OTU) tables. A diversity measure, including the observed species number (97% sequence identity threshold) and Chao1, Shannon, and phylogenetic diversity indexes, was calculated for the rarefied OTU tables.

Immunohistochemical measurements

Immunohistochemical staining analyses were conducted according to our published protocols [14]. Slides were incubated with primary antibodies, including beclin1 (1:600; MBL International), LC3 (1:600; MBL International), claudin-2 (1:500), occludin (1:200) and ZO-1 (1:200). The detailed information for LC-3, claudin-2, occludin and ZO-1 is presented in Table 1. Immune complexes were detected with the appropriate peroxidase-coupled secondary antibody and visualized using the Liquid DAB Plus Substrate Kit (Life Technologies, Carlsbad, CA, USA). Images were acquired under light microscopy by a blinded observer, and enumeration of positively stained cells was accomplished by counting 10 × 40 microscopic fields in six sections from six rats per group.

Dual immunofluorescence

Dual immunofluorescence was performed following the protocol published by our group [18]. Frozen sections (4 mm thick) were processed and incubated with primary antibodies, including LC3 and claudin-2, occludin, and ZO-1, as indicated in Table 1. Slides were analyzed using a Zeiss Axioplan 2 fluorescence microscope (Carl Zeiss, Thornwood, NY, USA) equipped with FITC (green), PE (red) and DAPI (blue) filter sets. All digital images were processed and merged using Photoshop software, v.6.0 (Adobe Systems, San Jose, CA, USA).

Western blot analysis

Western blot analysis was performed following a previously published protocol [14]. The following antibodies were used as primary antibodies: HMGB1 (1: 80, Shino-Test Corporation, Tokyo, Japan), Apaf-1 (Santa Cruz Biotechnology), caspase-3 (Santa Cruz Biotechnology), LC-3 (MBL International), beclin-1 (MBL International), claudin-1 (MBL International), p62 (BD Biosciences), claudin-2, occludin and ZO-1. The detailed information for LC-3, claudin-2, occludin and ZO-1 is presented in Table 1. Proteins were detected using the ECL Plus Western Blotting Detection System (Amersham Life Science, Braunschweig, Germany). All critical blot experiments were repeated at least three times. The relative intensities of the bands were evaluated to compare protein expression between groups by densitometry using Image-Pro Plus 6.0 (Media Cybernetics, MD, USA). The optical density (OD) levels from each sample were normalized to the OD of the corresponding β-actin samples.

Glutathione and glutathione disulfide measurements

The glutathione (GSH) and oxidized glutathione (GSSG) measurements were conducted using a commercially available assay (Glutathione Assay Kit II, Merck Chemicals, Hull, UK) as previously described [16]. In brief, homogenized supernatant fractions of intestinal tissues (1 mg) were collected and subjected to GSH and GSSG measurements using the Assay Cocktail reagents. The GSH/GSSG content is expressed as nmol/mg protein. Values are presented as the mean of three independent experiments ± SD.

Table 1 Paired antibodies for dual confocal immunofluorescence

Paired	Primary	Host	Catalog	Manufacturer	Secondary antibodies (invitrogen)
1	LC3	Mouse	M152-3	MBL International	Goat anti-mouse AlexaFluor 594
	Claudin-2	Rabbit	32-5600	Thermo Fisher	Goat anti-rabbit AlexaFluor 488
2	LC3	Mouse	M152-3	MBL International	Goat anti-mouse AlexaFluor 594
	Occludin	Rabbit	71-1500	Zymed Laboratories	Goat anti-rabbit AlexaFluor 488
3	LC3	Mouse	M152-3	MBL International	Goat anti-mouse AlexaFluor 594
	ZO-1	Rabbit	ab96587	Abcam	Goat anti-rabbit AlexaFluor 488

Intestinal permeability assessment

In vivo intestinal permeability was determined as previously described with minor modifications [19]. The day following ANP induction, mice were gavaged with 0.44 mg/g body weight of a 100 mg/ml solution of fluorescein isothiocyanate (FITC) conjugated to dextran (70 kDa; Sigma-Aldrich, St. Louis, MO, USA) in PBS (pH 7.4). Four hours later, animals were killed to collect whole blood (50 mL) and small intestines. Blood was allowed to clot overnight at 4 °C and subsequently centrifuged to collect serum. The serum fluorescence values were compared with serial dilutions of known FITC-dextran concentrations.

Amylase and lipase activities

Amylase and lipase activities in plasma (U/l) were measured by routine methods in our clinical chemistry laboratory via a two-step specific pancreas amylase assay (DiaSys Diagnostic Systems International, Holzheim, Germany).

Endotoxin assay

The levels of LPS were measured using photometric detection test kits (Beijing Jinshan Science and Technology Co., Ltd., Beijing, China) according to the manufacturer's protocol. The results were analyzed, and a cut-off point was set at 10 pg/mL according to the manufacturer's instructions.

Measurements of malonaldehyde (MDA), superoxide dismutase (SOD) and myeloperoxidase (MPO) in the intestine

Intestinal tissues were first homogenized in 5 mM butylated hydroxytoluene to prevent sample oxidation, and the intestinal malonaldehyde (MDA) content and superoxide dismutase (SOD) activity were determined in supernatants using the respective commercial kits according to the manufacturer's instructions as previously described. The MDA content in the intestine is expressed as nmol/mg protein content. The SOD activity in the intestine is expressed as U/mL. The results were normalized to the protein contents of the crude homogenates. The myeloperoxidase (MPO) activity was measured as described previously [20].

Statistical analysis

Statistical measurements were performed using SPSS software (SPSS, Inc., Chicago, IL, USA). The continuous parametric data shown in figures are expressed as the mean ± SD (standard deviation). Student's unpaired *t* test was used to determine differences between two groups. One-way analysis of variance (one-way ANOVA) multiple comparison tests were used to identify differences in mRNA expression, serum amylase levels and detailed histopathologic scores (e.g., edema and acinar necrosis). The statistical significance of the separation among PCoA score plots was assessed by multivariate analysis of the variance test. $p \leq 0.05$ was considered to indicate a statistically significant difference.

Results

HMGB1 inhibition ameliorated the severity of ANP

Under histopathological evaluation, ANP was characterized by pancreatic hyperemia, edema, infiltration of neutrophils, mass of dissolved acinar cell membrane and necrosis (Fig. 1a). HMGB1 inhibition significantly alleviated pancreatic injury by over 50%, as revealed by the histopathological scores (Fig. 1b, c). Similarly, HMGB1 inhibition significantly affected plasma amylase and lipase during pancreatic injury (Fig. 1d, e).

Western blot analysis revealed that HMGB1 protein expression was also elevated at 12 h after induction of ANP compared with that in the control group (Fig. 1f, g). Consistent with the HMGB1 protein level, HMGB1 mRNA increased in ANP-damaged pancreatic tissues compared with the control (Fig. 1h) and was significantly positively correlated with the HMGB1 protein level. Because the HMGB1 inhibitor is an antibody, its inhibition efficiency exhibited through downregulation of the expression level.

HMGB1 inhibition protected against microbiome changes in ANP

Next, the extent of BT was evaluated with HMGB1 inhibition. As indicated in Fig. 2a–c, HMGB1 inhibition suppressed BT across the intestinal barrier into mesenteric lymph nodes and the spleen, as induced by ANP. Furthermore, serum LPS exhibited a similar tendency compared to BT (Fig. 2d).

The qualitative composition of the intestinal microbiome was investigated by qPCR using universal 16S rRNA bacterial primer sets. The total number of intestinal microbiomes in mice with experimental ANP exhibited a significant decrease compared with the control (Fig. 2e). The richness of microbial species, as estimated by the Chao1 estimator (Fig. 2f), presented a significant decrease in the ANP group compared to that in the control group, with HMGB1 inhibition preserving a greater richness of microbial species. Likewise, the Shannon index and Simpson index demonstrated similar patterns, suggesting that HMGB1 inhibition reversed the loss of microbiome diversity in ANP rats.

The similarities (principle component analysis, PCA) between the gut microbiota composition of the different

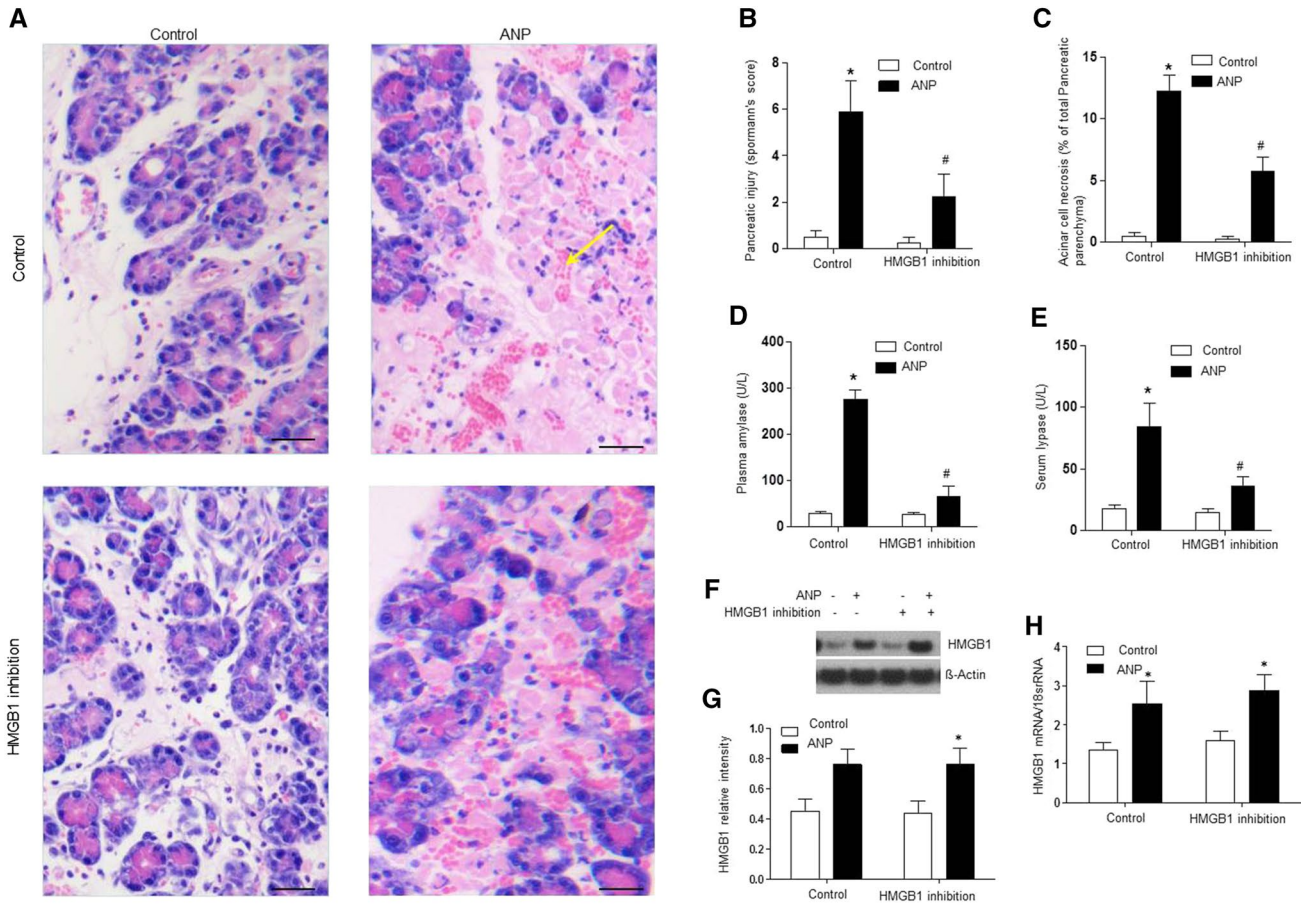

Fig. 1 HMGB1 inhibition reduces tissue damage associated with acute pancreatitis. Histological sections of pancreas obtained from rats 12 h after ANP induction, treated as indicated, were subjected to H&E staining for morphometric analyses, as described previously ($n=6$ animals, 12 fields/animal). **a** Representative ANP showing a severe degree of pancreatic damage characterized with the infiltration of inflammatory cells, widespread edema, and focal necrosis (arrowhead). Scale bar = 50 mm. Morphometric analyses revealing that treatment with HMGB1 neutralizing antibody ameliorates the changes of Spormann's score (**b**) and the acinar cell necrosis percentage (**c**), which reduced pancreatic injury of ANP. Measurement of plasma amylase (**d**) and lipase (**e**) was performed in rats treated as indicated. Columns: average values of six independent experiments per groups; bars: −SD; $^{*}p<0.05$ compared with the corresponding sham operation control, $^{\#}p<0.05$ compared with the corresponding ANP group, one-way ANOVA. **f** mRNA of HMGB1 in rats treated as indicated, expressed relative to the housekeeping gene 18 s rRNA. Columns: average values of a minimum of three independent experiments; bars: −SD. $^{*}p<0.05$ compared with the corresponding sham operation control, $^{\#}p<0.05$ compared with the corresponding ANP group (one-way ANOVA). **g** Immunoblot analysis revealing the pancreatic protein levels of HMGB1 in rats treated as indicated. A representative example from a minimum of three independent experiments is shown. **h** The quantitative data of the relative intensity for immunoblot analysis were calculated relative to β-actin. Columns: average values of three independent experiments; bars: −SD. $^{*}p<0.05$ compared with the corresponding sham operation control, $^{\#}p<0.05$ compared with the corresponding ANP group (one-way ANOVA). *ANOVA* analysis of variance, *HMGB1* high-mobility group box-1

samples (Fig. 2g) showed that the treated and control groups clustered separately and that the control samples clustered more tightly than the ANP samples. Control and HMGB1 inhibition for ANP appeared to cluster together, while the ANP samples clustered separately (Fig. 2g). Thus, the microbiota of animals with ANP was characterized by remarkably higher differences in overall composition with respect to the microbiota of animals with HMGB1 inhibition of ANP compared to control animals.

HMGB1 inhibition relieved intestinal mucosal injury in ANP rats

ANP intestinal mucosal injury (Fig. 3a) was characterized under light microscopy by parenchyma hemorrhage, villus denudation, infiltration of inflammatory cells, and lamina propria disintegration, with the HMGB1 neutralizing antibody significantly decreased in the associated-ANP mucosal injury (Fig. 3b).

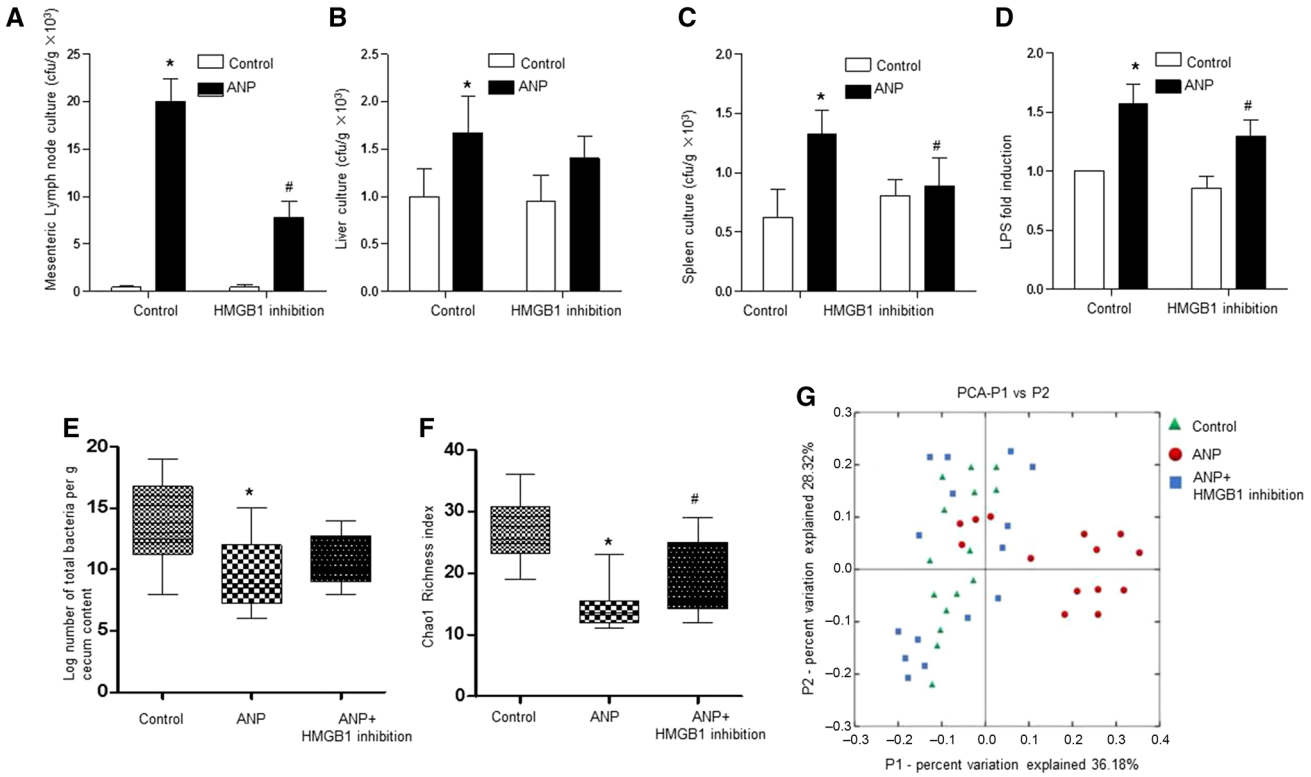

Fig. 2 HMGB1 inhibition affects bacterial translocation and the gut microbiota in ANP. Quantification of bacterial growth from mesenteric lymph nodes (**a**), the liver (**b**), and the spleen (**c**) of rats 12 h after ANP induction under the indicated conditions. The data are presented as the means of a minimum of three independent experiments. Bars: −SD. $^{*}p<0.05$ compared with the corresponding sham operation control, $^{\#}p<0.05$ compared with the corresponding ANP group (one-way ANOVA). **d** Endotoxin levels (LPS) relative to the sham operation control are presented ($n=5$–10 animals per groups). $^{*}p<0.05$ compared with the corresponding sham operation control, $^{\#}p<0.05$ compared with the corresponding ANP group (one-way ANOVA). **e** The total population of intestinal microbes detected by qPCR in mice with the indicated treatments. **f** The Chao1 richness index evaluated in mice with the indicated treatments. The horizontal lines indicate mean values. $^{*}p<0.05$ compared with the corresponding control groups (one-way ANOVA), $^{\#}p<0.05$ compared with the corresponding ANP group (one-way ANOVA). **g** PCA of the cecal microbiota in different experimental groups. Each symbol represents one microbiota (dot)

Along with the increase in intestinal mucosal injury, mucosal apoptosis and intestinal mucosal permeability were increased in mice with ANP and were reversed by HMGB1 inhibition (Fig. 3c–e). Furthermore, the expression of the apoptosis marker caspase-3, as determined by SDS-PAGE (Fig. 3f–g), was significantly attenuated in intestinal tissue by HMGB1 inhibition.

Oxidative stress induced by ANP could be eliminated by HMGB1 inhibition

Because they could be used to measure lipid peroxidation, we next measured the increase of the lipid peroxidation markers MDA, MPO and SOD in intestinal tissue that exhibited oxidative cellular damage caused by ANP, and this increasing trend could be normalized with HMGB1 inhibition (Fig. 4a–c).

We further investigated whether mucosal oxidized glutathione (GSSG) and GSH accounted for the aforementioned mucosal lipid peroxidation in ANP. As indicated in Fig. 4d–f, the GSH levels increased twofold in ANP compared with control animals, and HMGB1 inhibition did prevent this increase. In experimental ANP mice, the GSSG/GSH ratio increased to 1.4 from approximately 0.2 in the control (Fig. 4f), indicating severe intestinal oxidative stress, and HMGB1 inhibition was found to alleviate the GSSG/GSH ratio by approximately 50%, suggesting an antioxidative capacity of the anti-HMGB1 antibody.

Anti-HMGB1 antibody prevented disruption of tight junction proteins

The expression of multiple TJ proteins was further investigated to explore ileal mucosal barrier dysfunction, which revealed a trend toward an increase in these proteins compared with controls. We observed significant changes in the levels of claudin-1, claudin-2 and occludin, but not in the level of ZO-1, in the ANP group via western blot

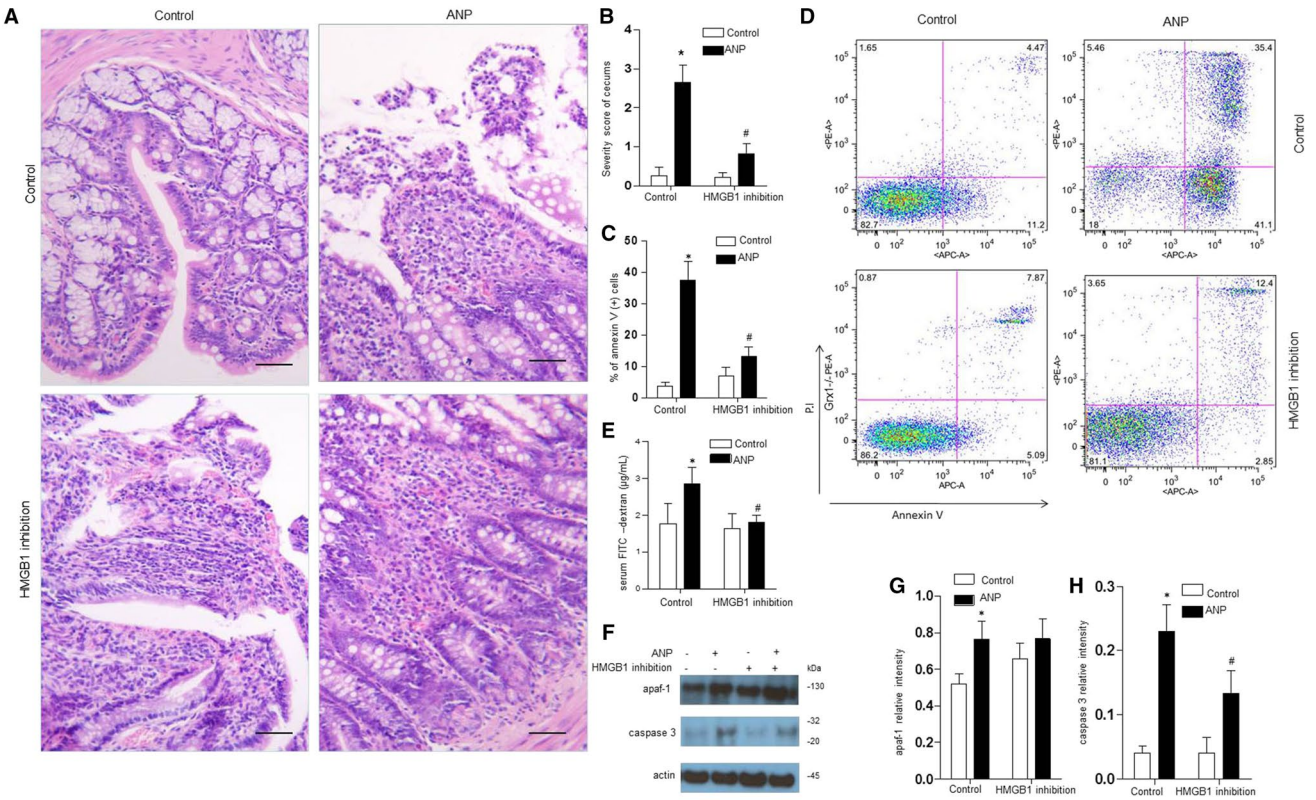

Fig. 3 HMGB1 blockade attenuates acute pancreatitis-associated intestinal mucosal damage. **a** Histologic sections of intestinal tissues obtained from rats treated as indicated on post-operative day 1 were subjected to H&E staining for morphometric analyses ($n=6$ animals, 12 fields/animal). Representative H&E stainings of three independent replicate coverslips per condition are shown (scale bars 50 μm). **b** Histogram of the severity scores of the terminal ileums ($n=10$) graded microscopically by two independent pathologists. The data are presented as the mean ± SD. $^{*}p<0.05$ compared with the corresponding sham operation control, $^{\#}p<0.05$ compared with the corresponding ANP group, one-way ANOVA. **c** Histogram of multiple flow cytometry experiments; the columns represent the mean percentage of Annexin V-positive cells from three independent experiments. The data are presented as the mean ± SD, $^{*}p<0.05$ compared with the corresponding sham operation control, $^{\#}p<0.05$ compared with the corresponding ANP group, one-way ANOVA. **d** Representative flow cytometry diagrams of at least three independent experiments are presented. **e** The concentration of serum FITC-dextran from rats 12 h after ANP induction treated as indicated. The values presented as the mean ± SD. A minimum of three independent experiments were performed. $^{*}p<0.05$ compared with the corresponding sham operation control, $^{\#}p<0.05$ compared with the corresponding ANP group, one-way ANOVA. **f** Immunoblotting analysis of Apaf-1 and caspase-3 proteins in intestinal homogenates from rats 12 h after ANP induction treated as indicated. The data are representative of three independent experiments with the protein weights indicated (in kDa). β-actin was used as a loading control. The quantitative intensities of Apaf-1 (**g**) and caspase3 (**h**) were calculated relative to β-actin. Columns: average values of three independent experiments; bars: SD. $^{*}p<0.05$ compared with the corresponding sham operation control, $^{\#}p<0.05$ compared with the corresponding ANP group, one-way ANOVA

analysis (Fig. 5a–d). Furthermore, administration of the anti-HMGB1 antibody significantly downregulated some of the TJ proteins (Fig. 5b–d).

The pore-forming TJ protein claudin-2 was only barely detectable in the immunohistochemical examination of control animals, whereas rats from the ANP group showed intense staining of claudin-2 from the crypts to the surface of the small intestine (Fig. 5e). The anti-HMGB1 antibody could reverse this pattern of expression in ANP rats. In contrast to claudin-2, the expression and distribution of occludin and ZO-1 were similar in control and ANP tissues (Fig. 5e).

HMGB1 inhibition decreased intestinal expression of autophagy regulators

Previous work has indicated that autophagy contributes to the pathogenesis of intestinal injury. Next, we determined AP-associated intestinal autophagy, as indicated by the turnover of the beclin-1 and LC3 or SQSTM1/p62 contents using immunoblotting to monitor autophagy flux. Only a low basal level expression of beclin1 and LC3 was detected in the control. The opposite expression pattern of SQSTM1/p62 to beclin 1 and LC3 verified autophagy activation in ANP rats. Furthermore, HMGB1 inhibition exhibited an impaired autophagy flux, with

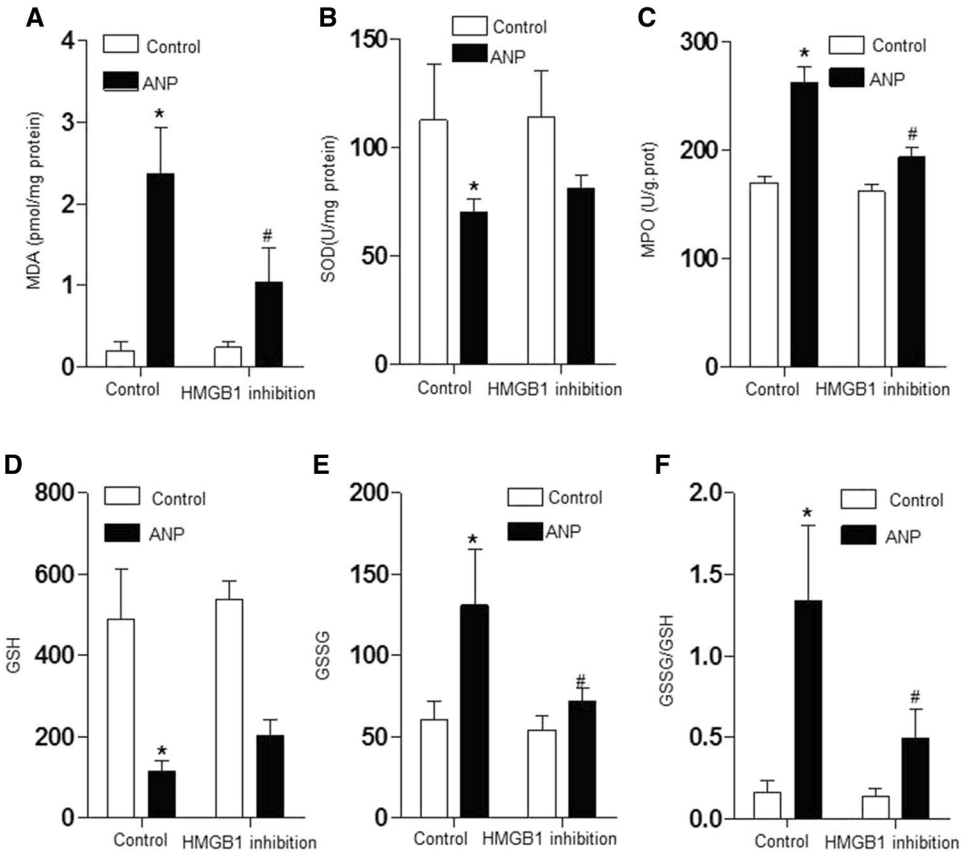

Fig. 4 HMGB1 inhibition reduces acute pancreatitis-induced oxidative stress in intestinal tissues. The levels of MDA (**a**), SOD (**b**), MPO (**c**), GSH (**d**), and GSSG (**e**) and the GSH to GSSG ratio (**f**) in intestinal homogenates from rats 12 h after ANP induction treated as indicated were determined. The columns represent the average values of three independent experiments; bars, SD. $^{*}p < 0.05$ compared with the corresponding sham operation control, $^{\#}p < 0.05$ compared with the corresponding ANP group, one-way ANOVA. **g** mRNA expression of TLR4 relative to β-actin mRNA was evaluated in intestinal homogenates from rats 12 h after ANP induction treated as indicated

relatively low levels of both Beclin 1 and LC3II (Fig. 6a–c) and an increase of SQSTM1/p62, suggesting a protective effect of autophagy with HMGB1 inhibition against ANP-associated injury.

The expression of LC3 was almost undetectable in the control, was clearly visible in intestinal epithelial cells of rats exposed to ANP (Fig. 6d), and was reduced in ANP rats exposed to HMGB1 inhibition. The same results were found for beclin1 expression (Fig. 6d).

The functional relationship between the autophagy regulator LC3 and tight junction proteins was further investigated using the dual immunostaining method. Typical images of dual-stained LC3 and TJs (arrows) of the intestinal tissues are shown in Fig. 7a. A higher degree of colocalization of LC3 and TJs was revealed in the merged images from intestinal tissues with ANP (Fig. 7a, b). Additionally, a relatively low degree of colocalization of the autophagy regulator LC3 and tight junction proteins was observed with anti-HMGB1 antibody administration.

Discussion

The present study demonstrated that HMGB1 blockade using an anti-HMGB1 neutralizing antibody ameliorated the severity of ANP through preventing intestinal permeability, which was associated with the transport of dangerous bacteria and/or toxins through the intestinal wall. HMGB1 inhibition ameliorated the disruption of TJs and autophagy exhibited in ANP and adjusted oxidative stress to maintain the internal environment. These observations suggested, for the first time, that HMGB1 plays a critical role in the pathogenesis of ANP by affecting intestinal permeability and autophagy.

As HMGB1 is an essential cytokine that modulates the activation of inflammation, HMGB1 blockade has been proposed to be a novel strategy to inhibit the inflammatory process in multiple pathologic processes, including infectious diseases [21], acute lung injury [22], brain injury

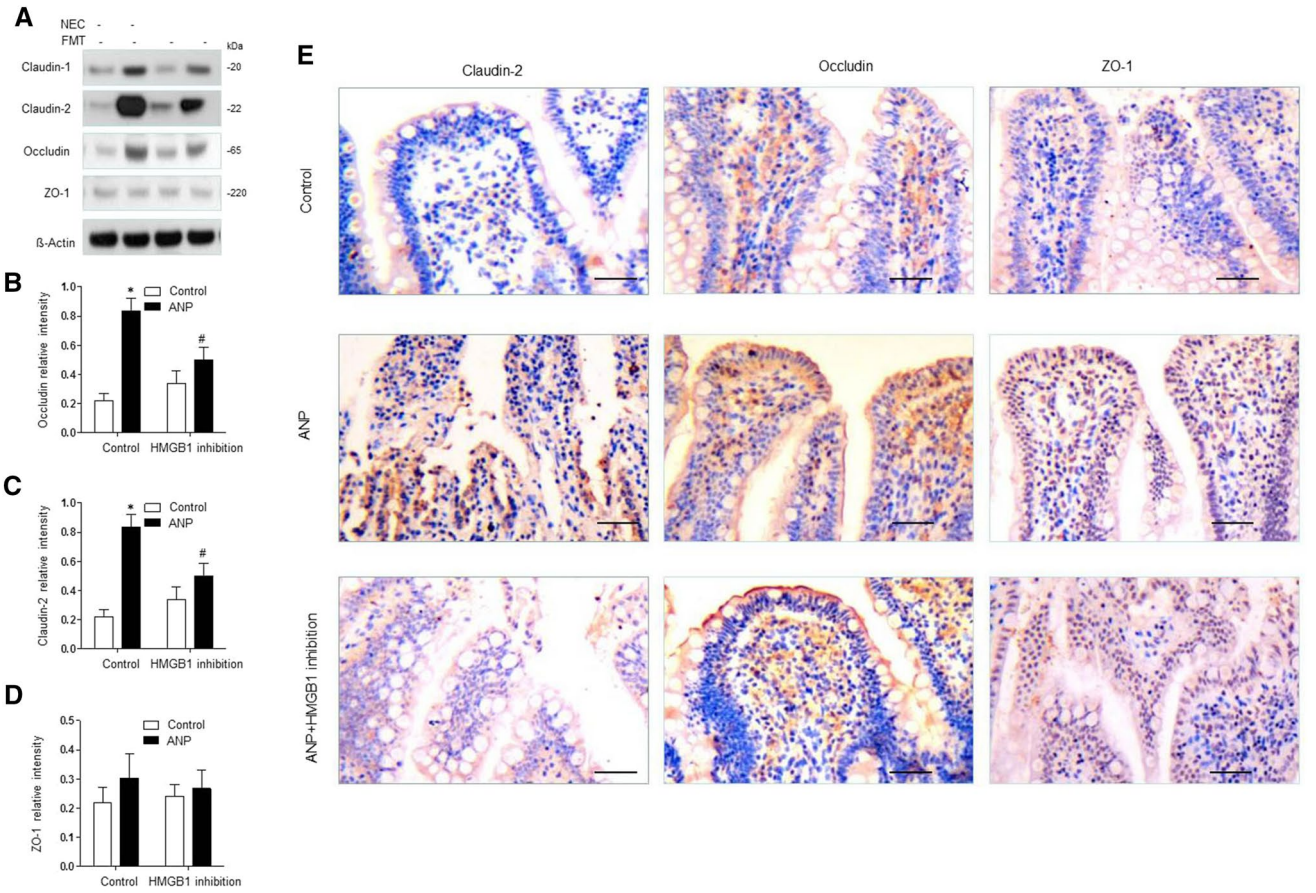

Fig. 5 HMGB1 inhibition prevents the disruption of tight junction proteins. **a** Immunoblotting analysis of occludin, claudin-1, claudin-2 and ZO-1 in intestinal homogenates from experimental ANP rats 12 h after ANP induction treated as indicated. The data are representative of three independent experiments, with the protein weights indicated (in kDa). β-actin was used as a loading control. The quantitative intensities of occludin (**b**), claudin-2 (**c**), ZO-1 (**d**) were calculated relative to β-actin. Columns: average values of three independent experiments; bars: SD. $^{*}p<0.05$ compared with the corresponding sham operation control, $^{\#}p<0.05$ compared with the corresponding ANP group, one-way ANOVA. **e** Immunohistochemistry staining of occludin, claudin-2 and ZO-1 in intestinal sections from experimental ANP rats 12 h after ANP induction treated as indicated. Representative staining of three independent replicate coverslips per condition are shown. Bar = 50 μm

[23], liver disease [24], intestinal barrier disruption [25], and precancerous lesions [26]. Acting as a key mediator of inflammation, HMGB1 also seems to be associated with pancreatic tissue damage and intestinal barrier injury [27]. In the present study, we observed that the anti-HMGB1 antibody could eliminate the severity of ANP, with edema, acinar cell necrosis, fat necrosis, and perivascular inflammation resolved in pancreatic tissues exposed to the anti-HMGB1 antibody.

The severity and mortality of AP resulted from the infection process of pancreatic necrosis, which was considered to mainly result from the pathophysiological role of the gastrointestinal tract, with BT and endotoxin permeation crossing the intestinal barrier. The resulting sepsis was the important factor that initiated and aggravated organ dysfunction syndrome (MODS) involved in ANP [28–30]. In preventing ANP development, intestinal barrier maintenance is of great importance to prevent intestinal mucosal injury and cecal bacterial overgrowth and decrease gut motility and compromised host immune functions [31]. The present study further confirmed that BT interruption and gut barrier dysfunction amelioration by HMGB1 blockade could eventually alleviate the severity of ANP. In the present study, obvious histological lesions with vascular dilation and congestion were indicated in the small intestine with ANP, and the alleviation of ileal mucosal injury and intestinal permeability, as well as decreased endotoxin levels, was observed after the administration of the anti-HMGB1 antibody. We also found fewer pancreatic super infections in HMGB1 antibody-administered rats than in control animals.

The structure of the intestinal microbiota is sparse during the early stages of ANP, suggesting that intestinal colonization might be affected by the pathogenesis of ANP [32, 33], which is associated with the initiation of intestinal

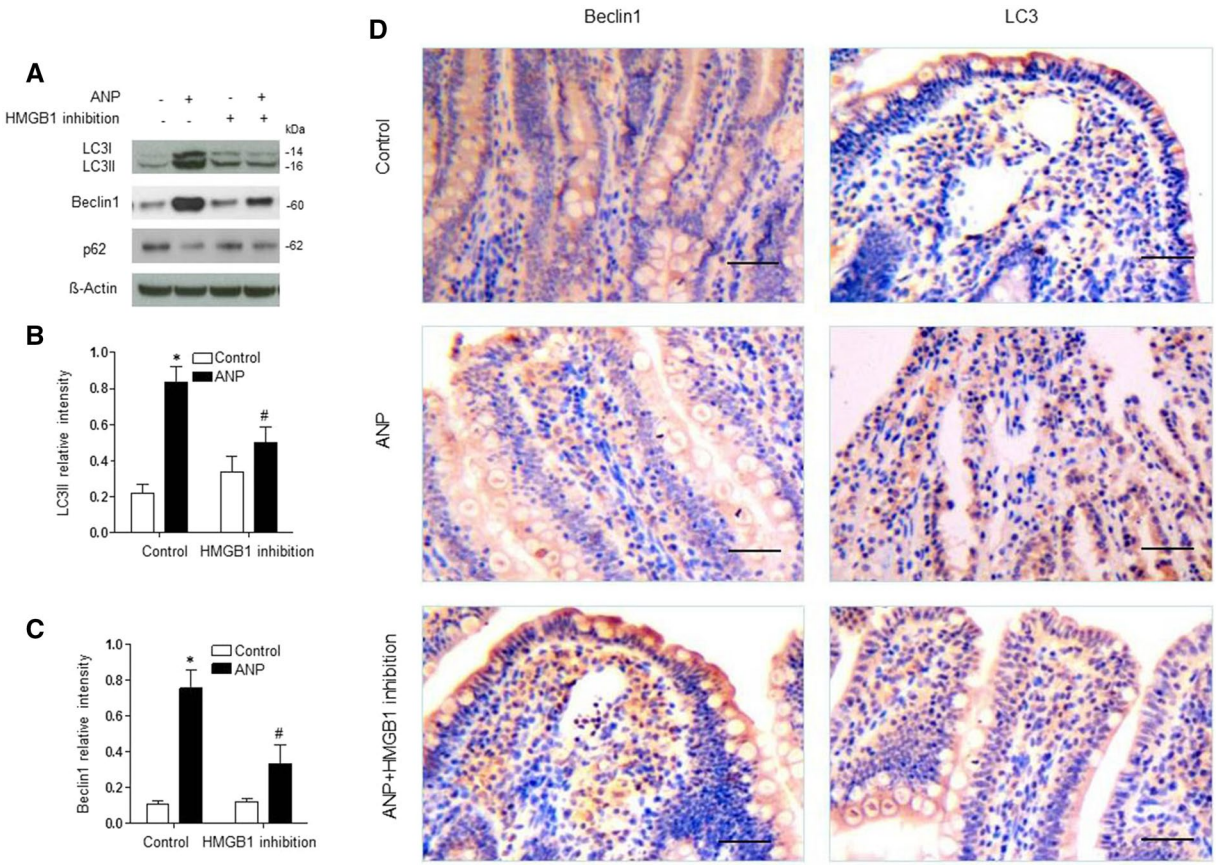

Fig. 6 Effect of HMGB1 inhibition on autophagy in the ileum of experimental ANP rats. **a** Immunoblotting analysis of the beclin 1, LC3 and p62 proteins in intestinal homogenates from experimental ANP rats 12 h after ANP induction treated as indicated. The data are representative of three independent experiments, with the protein weights indicated (in kDa). β-actin was used as a loading control. The quantitative intensities of beclin 1 (**b**) and LC3 (**c**) were calculated relative to β-actin. Columns: average values of three independent experiments; bars: SD. $^{*}p<0.05$ compared with the corresponding sham operation control, $^{\#}p<0.05$ compared with the corresponding ANP group, one-way ANOVA. **d** Immunohistochemistry staining of beclin 1 and LC3 in intestinal sections from experimental ANP rats 12 h after ANP induction treated as indicated. LC3B was present in the cytoplasm of intestinal epithelial cells. Representative stainings of three independent replicate coverslips per condition are shown. Bar = 50 μm

inflammation. Our study demonstrated that both the number and diversity of gut microbiota were disturbed in the cecum with ANP. HMGB1 inhibition accelerated the re-establishment of the disruption of intestinal microbial homeostasis in the intestine to the previous level, which in turn, prevented intestinal BT. In experimental ANP models, some Bacteroides and Bacillus species that had been previously suggested to protect against disease development were maintained with the HMGB1 inhibition.

Oxidative stress is believed to play an important role in many inflammatory illnesses, including ANP, which should be the mechanism of BT [34]. Under physiological conditions, ROS are captured by sufficient amounts of antioxidants. A lack of sufficient antioxidative reserve leads to oxidative stress with increased-ROS production. GSH plays a pivotal role in preventing oxidative damage and maintaining the mucosal barrier through maintenance of the redox balance (expressed as GSH/GSSG ratios) [16]. Indeed, our data showed that ANP induced oxidative damage to lipid membranes, as revealed by the MDA and SOD levels, which was prevented by HMGB1 inhibition, providing further evidence that oxidative stress exerts deleterious effects on the mucosal barrier function.

Several mechanisms for intestinal permeability have been proposed, including intestinal epithelial cell apoptosis and/or tight junction integrity disruption [35, 36]. During ANP, oxidative stress might disrupt the structure of TJs, which determine the epithelial barrier properties. In the present study, disruption of TJs resulted in increased mucosal permeability, promoting the release of luminal LPS, bacteria, and proinflammatory cytokines. Previous reports have suggested that claudin-1 distribution alternation and claudin-2 upregulation are present in AP [37] and are also found in inflammatory bowel disease [38] and NEC [39]. Further, immunostaining in the current study revealed that HMGB1-antibody administration maintained

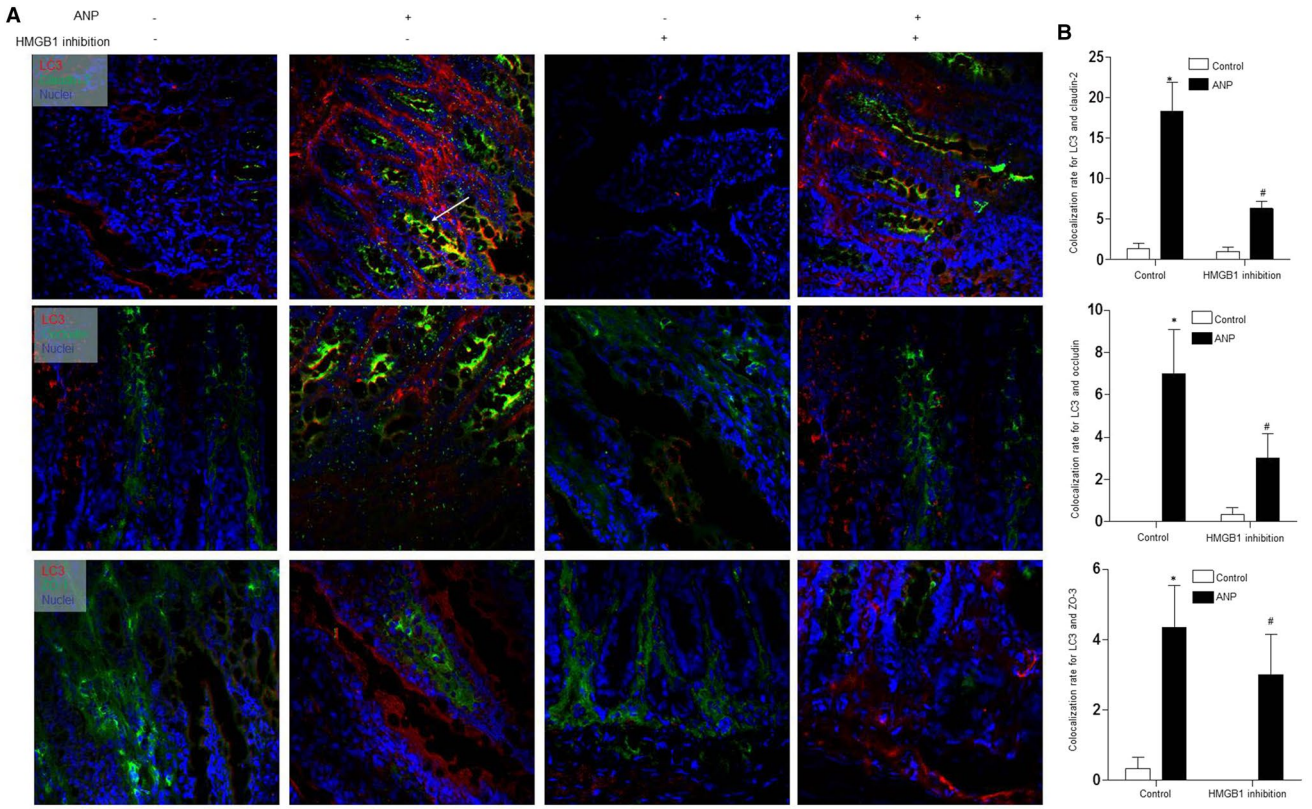

Fig. 7 Merged immunofluorescent colocalization of the autophagy marker LC3 (red) and tight junction proteins, occludin, claudin-2 and ZO-1 (green) in intestinal sections from experimental ANP rats 12 h after ANP induction treated as indicated. The images (left column in each group) also show DAPI nuclear staining (blue). Colocalization in the intestinal epithelium (yellow, double positive cells, arrowheads) on the merged image is indicated. Representative patterns of the staining of three independent replicate coverslips per condition are shown. Bar = 100 µm. **b** The average number of colocalized cells per 100 cells in 20 random photomicrographs of 4 sections per sample of at least 4 independently acquired samples from each group. Columns: average values of three independent experiments; bars: SD. $^{*}p < 0.05$ compared with the corresponding sham operation control, $^{\#}p < 0.05$ compared with the corresponding ANP group, one-way ANOVA (color figure online)

a normal distribution of TJ proteins, including claudin-1 and claudin-2.

Autophagy plays an important role in many biological activities through removing damaged cells and proteins [40]. Whether autophagy has a function in intestinal mucosal injury is pending description, although recent studies have attempted to investigate the role of autophagy in intestinal development and diseases [41]. Additionally, the connection between tight junction integrity and autophagy has not yet been addressed. Our data clearly demonstrated an increased mucosal expression of beclin-1 and LC3 in ANP-associated intestinal injury. In the current setting, increased autophagy was associated with intestinal permeability and subsequent intestinal injury. Uncontrolled autophagy destroyed the structure of TJ proteins due to excessive degradation, ultimately leading to apoptosis, and this process was reversed by HMGB1 inhibition. These findings require additional experiments to determine the pathophysiological relevance of autophagy and intestinal permeability in ANP.

In summary, our findings provide new insights into the role of HMGB1 inhibition in rats with experimental ANP. We demonstrate that the protective effect of HMGB1 blockade on ANP may be due, at least in part, to the elimination of oxidative stress and preservation of TJ molecular expression, which should enhance intestinal barrier function. These results provide a potential therapeutic approach for intestinal mucosal barrier dysfunction in ANP through HMGB1 manipulation.

Acknowledgements We thank Prof. Bailin Chen for providing technical assistance and for insightful discussions during the preparation of the manuscript. We thank Dr. Xiaoyong Zhang at the Wistar Institute, USA, for help with the linguistic revision of the manuscript.

Author contributions LH bred animals and constructed the ANP model. DZ designed the experiments, performed the statistical

analyses, measured the data, and revised the manuscript. CG analyzed and interpreted the data and wrote the paper.

Funding The research was supported by National Natural Science Foundation of China (Grant Nos: 81270448, 81470890).

Compliance with ethical standards

Conflict of interest No potential conflicts of interest relevant to this article are reported.

References

1. Petrov MS, Shanbhag S, Chakraborty M, Phillips AR, Windsor JA. Organ failure and infection of pancreatic necrosis as determinants of mortality in patients with acute pancreatitis. Gastroenterology. 2010;139:813–20.
2. Moran RA, Jalaly NY, Kamal A, Rao S, Klapheke R, James TW, Kambhampati S, Makary MA, Hirose K, Kumbhari V, Stein EM, Khashab MA, Lennon AM, Kalloo AN, Zaheer A, Hernaez R, Singh VK. Ileus is a predictor of local infection in patients with acute necrotizing pancreatitis. Pancreatology. 2016;16:966–72.
3. Chen X, Zhao HX, Bai C, Zhou XY. Blockade of high-mobility group box 1 attenuates intestinal mucosal barrier dysfunction in experimental acute pancreatitis. Sci Rep. 2017;7:6799.
4. Garg PK, Madan K, Pande GK, Khanna S, Sathyanarayan G, Bohidar NP, Tandon RK. Association of extent and infection of pancreatic necrosis with organ failure and death in acute necrotizing pancreatitis. Clin Gastroenterol Hepatol. 2005;3:159–66.
5. Rau BM, Bothe A, Kron M, Beger HG. Role of early multisystem organ failure as major risk factor for pancreatic infections and death in severe acute pancreatitis. Clin Gastroenterol Hepatol. 2006;4:1053–61.
6. Nighot M, Al-Sadi R, Guo S, Rawat M, Nighot P, Watterson MD, Ma TY. Lipopolysaccharide-induced increase in intestinal epithelial tight permeability is mediated by toll-like receptor 4/myeloid differentiation primary response 88 (MyD88) activation of myosin light chain kinase expression. Am J Pathol. 2017;187:2698–710.
7. Wang Y, Mumm JB, Herbst R, Kolbeck R, Wang Y. IL-22 increases permeability of intestinal epithelial tight junctions by enhancing claudin-2 expression. J Immunol. 2017;199:3316–25.
8. Wang N, Han Q, Wang G, Ma WP, Wang J, Wu WX, Guo Y, Liu L, Jiang XY, Xie XL, Jiang HQ. Resveratrol protects oxidative stress-induced intestinal epithelial barrier dysfunction by upregulating heme oxygenase-1 expression. Dig Dis Sci. 2016;61:2522–34.
9. Oliver SR, Phillips NA, Novosad VL, Bakos MP, Talbert EE, Clanton TL. Hyperthermia induces injury to the intestinal mucosa in the mouse: evidence for an oxidative stress mechanism. Am J Physiol Regul Integr Comp Physiol. 2012;302:R845–53.
10. Tang Y, Zhao X, Antoine D, Xiao X, Wang H, Andersson U, Billiar TR, Tracey KJ, Lu B. Regulation of posttranslational modifications of HMGB1 during immune responses. Antioxid Redox Signal. 2016;24:620–34.
11. Kim HY, Park SY, Lee SW, Lee HR, Lee WS, Rhim BY, Hong KW, Kim CD. Inhibition of HMGB1-induced angiogenesis by cilostazol via SIRT1 activation in synovial fibroblasts from rheumatoid arthritis. PLoS One. 2014;9:e104743.
12. Sawa H, Ueda T, Takeyama Y, Yasuda T, Shinzeki M, Nakajima T, Kuroda Y. Blockade of high mobility group box-1 protein attenuates experimental severe acute pancreatitis. World J Gastroenterol. 2006;12:7666–70.
13. Xu GF, Guo M, Tian ZQ, Wu GZ, Zou XP, Zhang WJ. Increased of serum high-mobility group box chromosomal protein 1 correlated with intestinal mucosal barrier injury in patients with severe acute pancreatitis. World J Emerg Surg. 2014;9:61.
14. Deng WS, Zhang J, Ju H, Zheng HM, Wang J, Wang S, Zhang DL. Arpin contributes to bacterial translocation and development of severe acute pancreatitis. World J Gastroenterol. 2015;21:4293–301.
15. Schmidt J, Rattner DW, Lewandrowski K, Compton CC, Mandavilli U, Knoefel WT, Warshaw AL. A better model of acute pancreatitis for evaluating therapy. Ann Surg. 1992;215:44–56.
16. Li X, Li X, Shang Q, Gao Z, Hao F, Guo H, Guo C. Fecal microbiota transplantation (FMT) could reverse the severity of experimental necrotizing enterocolitis (NEC) via oxidative stress modulation. Free Radic Biol Med. 2017;108:32–43.
17. Yan AW, Fouts DE, Brandl J, Stärkel P, Torralba M, Schott E, Tsukamoto H, Nelson KE, Brenner DA, Schnabl B. Enteric dysbiosis associated with a mouse model of alcoholic liver disease. Hepatology. 2011;53:96–105.
18. Wang J, Bao L, Yu B, Liu Z, Han W, Deng C, Guo C. Interleukin-1β promotes epithelial-derived alveolar elastogenesis via αvβ6 integrin-dependent TGF-β activation. Cell Physiol Biochem. 2015;36:2198–216.
19. Vétizou M, Pitt JM, Daillère R, Lepage P, Waldschmitt N, Flament C, Rusakiewicz S, Routy B, Roberti MP, Duong CP, Poirier-Colame V, Roux A, Becharef S, Formenti S, Golden E, Cording S, Eberl G, Schlitzer A, Ginhoux F, Mani S, Yamazaki T, Jacquelot N, Enot DP, Bérard M, Nigou J, Opolon P, Eggermont A, Woerther PL, Chachaty E, Chaput N, Robert C, Mateus C, Kroemer G, Raoult D, Boneca IG, Carbonnel F, Chamaillard M, Zitvogel L. Anticancer immunotherapy by CTLA-4 blockade relies on the gut microbiota. Science. 2015;350:1079–84.
20. Yu B, Li X, Wan Q, Han W, Deng C, Guo C. High-mobility group box-1 protein disrupts alveolar elastogenesis of hyperoxia-injured newborn lungs. J Interferon Cytokine Res. 2016;36:159–68.
21. Yu R, Yang D, Lei S, Wang X, Meng X, Xue B, Zhu HL. HMGB1 promotes hepatitis C Virus replication by interaction with stem-loop 4 in the viral 5′ untranslated region. J Virol. 2015;90:2332–44.
22. Lan KC, Chao SC, Wu HY, Chiang CL, Wang CC, Liu SH, Weng TI. Salidroside ameliorates sepsis-induced acute lung injury and mortality via downregulating NF-κB and HMGB1 pathways through the upregulation of SIRT1. Sci Rep. 2017;7:12026.
23. Walker LE, Frigerio F, Ravizza T, Ricci E, Tse K, Jenkins RE, Sills GJ, Jorgensen A, Porcu L, Thippeswamy T, Alapirtti T, Peltola J, Brodie MJ, Park BK, Marson AG, Antoine DJ, Vezzani A, Pirmohamed M. Molecular isoforms of high-mobility group box 1 are mechanistic biomarkers for epilepsy. J Clin Invest. 2017;127:2118–32.
24. Yamamoto T, Ono T, Ito T, Yamanoi A, Maruyama I, Tanaka T. Hemoperfusion with a high-mobility group box 1 adsorption column can prevent the occurrence of hepatic ischemia-reperfusion injury in rats. Crit Care Med. 2010;38:879–85.
25. Sodhi C, Levy R, Gill R, Neal MD, Richardson W, Branca M, Russo A, Prindle T, Billiar TR, Hackam DJ. DNA attenuates enterocyte Toll-like receptor 4-mediated intestinal mucosal injury after remote trauma. Am J Physiol Gastrointest Liver Physiol. 2011;300:G862–73.
26. Shen X, Li WQ. High-mobility group box 1 protein and its role in severe acute pancreatitis. World J Gastroenterol. 2015;21:1424–35.
27. Luan ZG, Zhang H, Ma XC, Zhang C, Guo RX. Role of high-mobility group box 1 protein in the pathogenesis of intestinal barrier injury in rats with severe acute pancreatitis. Pancreas. 2010;39:216–23.

28. Ammori BJ. Role of the gut in the course of severe acute pancreatitis. Pancreas. 2003;26:122–9.
29. Ammori BJ, Fitzgerald P, Hawkey P, McMahon MJ. The early increase in intestinal permeability and systemic endotoxin exposure in patients with severe acute pancreatitis is not associated with systemic bacterial translocation: molecular investigation of microbial DNA in the blood. Pancreas. 2003;26:18–22.
30. Fritz S, Hackert T, Hartwig W, Rossmanith F, Strobel O, Schneider L, Will-Schweiger K, Kommerell M, Büchler MW, Werner J. Bacterial translocation and infected pancreatic necrosis in acute necrotizing pancreatitis derives from small bowel rather than from colon. Am J Surg. 2010;200:111–7.
31. Tadros T, Traber DL, Heggers JP, Herndon DN. Effects of interleukin-1alpha administration on intestinal ischemia and reperfusion injury, mucosal permeability, and bacterial translocation in burn and sepsis. Ann Surg. 2003;237:101–9.
32. Chen J, Huang C, Wang J, Zhou H, Lu Y, Lou L, Zheng J, Tian L, Wang X, Cao Z, Zeng Y. Dysbiosis of intestinal microbiota and decrease in paneth cell antimicrobial peptide level during acute necrotizing pancreatitis in rats. PLoS One. 2017;12:e0176583.
33. Huang C, Chen J, Wang J, Zhou H, Lu Y, Lou L, Zheng J, Tian L, Wang X, Cao Z, Zeng Y. Dysbiosis of intestinal microbiota and decreased antimicrobial peptide level in paneth cells during hypertriglyceridemia-related acute necrotizing pancreatitis in rats. Front Microbiol. 2017;8:776.
34. Abreu FF, Souza AC, Teixeira SA, Soares AG, Teixeira DF, Soares RC, Santana MT, Lauton Santos S, Costa SK, Muscará MN, Camargo EA. Elucidating the role of oxidative stress in the therapeutic effect of rutin on experimental acute pancreatitis. Free Radic Res. 2016;50:1350–60.
35. Chen WY, Wang M, Zhang J, Barve SS, McClain CJ, Joshi-Barve S. Acrolein disrupts tight junction proteins and causes endoplasmic reticulum stress-mediated epithelial cell death leading to intestinal barrier dysfunction and permeability. Am J Pathol. 2017;187:2686–97.
36. Yasuda T, Takeyama Y, Ueda T, Shinzeki M, Sawa H, Nakajima T, Kuroda Y. Breakdown of intestinal mucosa via accelerated apoptosis increases intestinal permeability in experimental severe acute pancreatitis. J Surg Res. 2006;135:18–26.
37. Lutgendorff F, Nijmeijer RM, Sandström PA, Trulsson LM, Magnusson KE, Timmerman HM, van Minnen LP, Rijkers GT, Gooszen HG, Akkermans LM, Söderholm JD. Probiotics prevent intestinal barrier dysfunction in acute pancreatitis in rats via induction of ileal mucosal glutathione biosynthesis. PLoS One. 2009;4:e4512.
38. Zeissig S, Bürgel N, Günzel D, Richter J, Mankertz J, Wahnschaffe U, Kroesen AJ, Zeitz M, Fromm M, Schulzke JD. Changes in expression and distribution of claudin 2, 5 and 8 lead to discontinuous tight junctions and barrier dysfunction in active Crohn's disease. Gut. 2007;56:61–72.
39. Bergmann KR, Liu SX, Tian R, Kushnir A, Turner JR, Li HL, Chou PM, Weber CR, De Plaen IG. Bifidobacteria stabilize claudins at tight junctions and prevent intestinal barrier dysfunction in mouse necrotizing enterocolitis. Am J Pathol. 2013;182:1595–606.
40. Ji L, Li L, Qu F, Zhang G, Wang Y, Bai X, Pan S, Xue D, Wang G, Sun B. Hydrogen sulphide exacerbates acute pancreatitis by over-activating autophagy via AMPK/mTOR pathway. J Cell Mol Med. 2016;20:2349–61.
41. Huett A, Xavier RJ. Autophagy at the gut interface: mucosal responses to stress and the consequences for inflammatory bowel diseases. Inflamm Bowel Dis. 2010;16:152–74.

Publisher's Note Springer Nature remains neutral with regard to jurisdictional claims in published maps and institutional affiliations.